In-situ structural degradation study of quadruple-cation perovskite solar cells with nanostructured charge transfer layer

In-situ structural degradation study of quadruple-cation perovskite solar cells with nanostructured charge transfer layer

Ivana Panžić[1], Vilko Mandić[,1], Jimmy Mangalam[2], Thomas Rath[2], Floren Radovanović-Perić[1], Mattia Gaboardi[3], Brend de Coen[4], Sara Bals[4], Nadine Schrenker[4]*

[1]Faculty of Chemical Engineering and Technology, University of Zagreb, Marulićev trg 20, 10000 Zagreb, Croatia
[2]Institute for Chemistry and Technology of Materials, NAWI Graz, Graz University of Technology, Stremayrgasse 9, 8010 Graz, Austria
[3]Elettra Sincrotrone Trieste S.C.p.A., Science Area Park, 4149 Basovizza, Trieste, Italy
[4]Faculty of Science, University of Antwerp, Groenenborgerlaan, 171, 2020 Antwerpen, Belgium

Abstract

We investigated the structural stability of perovskite solar cells (PSCs) in n-i-p configuration comprising a rubidium-caesium-methylammonium-formamidinium (Rb-Cs-MA-FA) lead iodide/bromide perovskite absorber, interfaced with nanostructured ZnO-nanorod (NR) or mesostructured (MS) TiO_2 electron transfer layers (ETL). An in-situ setup was established comprising synchrotron grazing incidence diffraction (GID) and Raman spectroscopy as a function of temperature under ambient and isothermal conditions; measurements of current-voltage (IV) characteristics and electron microscopic investigations were conducted discretely.

The aging of the solar cells was performed at ambient conditions or at elevated temperatures directly in the in-situ measurement setup. The diffraction depth profiling results point to different degradation rates for different ETLs; Moreover, electron microscopy and atomic force microscopy, as well as energy dispersive spectroscopy clarified surface conditions in terms of the extent of the degradation. Scanning transmission electron microscopy of lamellas, derived by dual beam microscopy, revealed that the origin of the degradation lay in the ETL/absorber interface. For the case of the nanostructured zincite, the perovskite absorber contained many voids, leading to the conclusion that the investigated quadruple perovskite absorber showed limited compatibility with ZnO NR ETL due to a higher number of defects. Morphological defects promoted the absorber degradation and nullified the advantages initially achieved by nanostructuring. The exchange of the ZnO NR ETL with MS TiO_2 improved the stability parameters of the absorber layer.

Keywords: In-situ structural degradation study; Synchrotron radiation GID; FIB-STEM; Quadruple cation PSC absorber; Nanostructured electron transfer layers; Absorber/ETL interface

Highlights

Quadruple perovskite absorbers facilitate efficiencies and mitigate degradation.
Nanostructured ETLs were varied, to affect the PSCs degradation.
Degradation circumstances were analysed by an in-situ synchrotron setup.
FIB-STEM definitively pointed to a problem at the absorber/ZnO NR interface.
Surface passivation could mitigate degradation at ZnO NR/perovskite interface.

1. Introduction

Perovskite solar cells (PSCs) are classified as emerging next-generation thin-film solar cells [**1**], and they are extremely prominent in the scientific literature. The considerable attention, that PSCs have been receiving, is a result of their main advantages: high efficiency (over 25 %), low cost, low recombination rate, tuneable band gap, high mobility of charge carriers, etc. [**1–4**]. There are, however, a few problems that hinder a wider and more commercial application of PSCs; the main problem being that hybrid perovskites are prone to both moisture and oxygen degradation, which limits their long-term stability [**5,6**]. Commonly used compositions are methylammonium (MA) and formamidinium (FA) lead iodide perovskites in planar device configuration ($MAFAPbI_3$) [**4,5**]. In order to address the previously mentioned degradation susceptibility, PSCs' development has been focused on multiple cation configuration. Namely, such compositions facilitate PSC stability. By compositional engineering, the absorbing layer was modified to include different cations: double (caesium and formamidinium), triple (caesium / methylammonium / formamidinium), and quadruple (rubidium / caesium / methylammonium / formamidinium) [**6–8**]. Band gap was commonly affected by substituting the halide part, i.e., substituting iodine with bromide [**9**]. Another point of view for the overall improvement of PSCs was found in excluding MA from the composition, since FA is thermally more stable, especially in combination with certain electron transport layers, which led to improved stability and lower hysteresis behaviour [**10**]. In addition to all of the mentioned strategies, several others have been employed to boost performance, such as doping, 2D/3D perovskite combinations, etc. [**11–14**].

Commonly, PSCs are assembled in so-called normal (n-i-p) or inverted (p-i-n) configuration, each of them showing both advantages and disadvantages in terms of efficiency vs. stability [**15**]. Organic-inorganic hybrid lead halide perovskites can repose in cubic, tetragonal, and hexagonal crystal lattices depending on the synthesis conditions [**20**], where solely the cubic structure is stable at room temperature, while the others are metastable high-temperature polymorphs [**20,21**]. Finding the optimal PSC configuration can be a main tool to prevent early degradation. For example, many reports [**16**] explain the role of the transport during the course of degradation from electrodes over the hole transport layer (HTL) to boundaries of the perovskite absorber of the PSCs in n-i-p configuration. Such focus is expected, as these (outside) layers are prone to ambient

[*]Correspondence: Vilko Mandić, Email: vmandic@fkit.unizg.hr, Tel: +385 1 4597 226, Marulićev trg 20, 10000 Zagreb, Croatia

moisture hydrolysis or are directly in the pathway of moisture diffusion [**17,18**]. Of the various candidates for ETLs and HTLs, TiO_2 and spiro-OMeTAD have been widely recognised. In comparison to TiO_2, ZnO has several advantages, such as the ability to be easily derived by low-cost, low-temperature methods, while retaining the needed wide band gap and long-term environmental stability [**19**].

However, we believe that the role of nanostructured ETLs has not been sufficiently monitored from the degradation point of view [**9,10**], particularly in the case of perovskite absorbers having more complex compositions. Namely, the role of the ETLs has been heavily exploited in terms of charge transfer efficiency increase [**24,25**]. Here, the nanostructuring emerged as the critical upgrade in the modern type of photovoltaic devices [**26**]. Again, only scarce reports exploit the role of the ETLs in the degradation process [**16**]. ETLs can be prepared via many methods, both physical and chemical methods [**27,28**], but here we have focused on the wet-chemistry techniques, where sol-gel processes [**29**] are beneficial for achieving homogeneous, cheap, nanostructured, multi-layered ETLs.

The development of the structural changes during aging is critically important in PSC systems, and this area is also under-investigated for the case of nanostructured transfer layers and complex composition perovskite absorbers. The studies reporting PSC degradation normally follow protocols for testing long-term stability in air at room temperature without encapsulation [**22**]. Commonly, PSCs are evaluated with respect to their efficiencies [**22,30**], because that is their most prominent property, which is closely related to the perovskite layer. However, stability is the property heavily related to adjacent and other layers [**31**]. Reports comparing and monitoring PSC aging at normal ambient conditions show that the light soaking is not a major reason for the poor stability of PSCs [**22**]. Available reports comparing and monitoring PSC aging at enhanced ambient conditions and elevated temperatures obviously suggest that several intrinsic factors, such as ion migration, electron-migrations, and interfacial reactions, play an important role in the degradation of the PSCs. [**23**]. In principle, the course and the outcome of the degradation include an interplay of multiple parameters, pointing out the necessity of relying on several quality indicators, which is surely device stability besides the PCE for the case of PSCs.

Different degradation pathways can take place in PSCs, including oxidation, photo oxidation, and decomposition [**32**]**.** If we focus on the active layer (the hybrid lead halide perovskite), the most common cause of loss of cell efficiency and long-term stability comes from the thermal decomposition of $MAPbI_3$, which decomposes in multiple steps to PbI_2, CH_3I, and NH_3 [**33**]**.** In addition, the HTL spiro-OMeTAD can also degrade at temperatures as low as 85 °C, because of the evaporation of the additives like tBP [**34**], leading to void formations in the layers. Furthermore, electrode materials such as gold and platinum can react with the halides present in the active layer under previously mentioned stressors like humidity, oxygen, and heat, and in some cases lead even to the formation of redox couples and corrosion [**35**]**.**

In general, it can be said that the dangling bonds at grain boundaries have to be passivated; the perovskite lattice must be structurally stable to endure all the possible stressors and avoid degradation. Thus, in addition to structural and chemical ways to tackle this, it is also necessary to consider the mechanical stress and strain that the thin-films have to withstand. Most perovskite films are under tensile stress, since, when cooling down, they cannot shrink as desired, due to the substrate they are on [**36**], making them prone to cracking and more susceptible to moisture- and heat-induced degradation.

It is not uncommon to observe in the literature that the importance of thorough multilayer structural characterisation is neglected. Reports on multi-technique characterisation of PSCs in an in-situ or in-operando setup are rare, especially using advanced characterisation techniques [**37**]. Namely, the advanced characterisation of SCs that are thin, multi-layered, and nanostructured is demanding, but we believe that this is a key area where deeper understanding of the materials and interfaces can lead to significant improvements.

The novelty of this paper lies in the investigation of the nanostructured ETLs as critical PSC constituents regarding device stability. The degradation stability of quadruple PSCs was studied through the perspective of comparing different nanostructured ETLs. For this purpose, we used a combination of a self-developed temperature-control unit and advanced structural depth profiling techniques to allow insight into the degradation process of a perovskite system that has shown to be one of the most stable, the quadruple cation perovskite. In the PSCs, we maintained the composition of humidity-susceptible constituents and focused on the influence of adjacent ETL layers; zincite nanorods (NR) and mesostructured (MS) titania. The results showed that zincite NR would benefit from passivation; therefore, titania-coated zinc oxide NRs, in a core-shell configuration are proposed.

2. Experimental

2.1. Synthesis

Glass/ITO transparent conducting oxide layers (TCL) substrates (15×15mm) were washed in detergent, acetone and IPA in consecutive 15 min ultrasonic stirring cycles, followed by 15 min ozonisation.

For the preparing of zincite vertical ordered nanorods as electron transfer layer (ETL), first an equimolar 0.025 M solution of ZnAc (zinc acetate dihydrate, $Zn(CH_3OO)_2{\cdot}2H_2O$, p.a. Sigma Aldrich, Netherlands) and MEA (monoethylamine, $CH_3CH_2NH_2$, p.a. Sigma Aldrich, Nederland) in EtOH (ethyl alcohol, CH_3CH_2OH, p.a. Sigma Aldrich, Netherlands) was prepared and spin coated (100 µL at 3000 rpm for 30 s, dried at 150 °C for 15 min) as the seed layer. The seed layer was mounted face down in a chemical bath reactor stirred at 150 rpm for 45 min at 83 °C. The reaction media consisted of 0.25M ZnN_6H (zinc nitrate hexahydrate, $Zn(NO_3)_2{\cdot}6H_2O$, p.a. Sigma Aldrich, Netherlands) and hexamine (hexamethylenetetraamine, $(CH_2)_6N_4$, p.a. Sigma Aldrich, Netherlands) dissolved at 40 °C in ultrasonic bath in MiliQ water. Prepared ZnO NR substrates were washed using MiliQ water and dried in nitrogen stream and thermally treated at 350 °C for 20 min on a hotplate.

For the preparing of mesoporous titania as ETL, firstly a compact layer of TiO_2 was deposited; 400 µL of acetylacetonate (p.a. Sigma Aldrich, USA) and 600 µL of titanium diisopropoxide (p.a. Sigma Aldrich, USA) were dissolved in 9 mL of ethanol. 50 µL of the prepared solution were spin coated on the glass/ITO substrates (4000 rpm, 2000 rpm s^{-1}, 30 s) for 30 s and dried on the hotplate

at 150 °C. To prepare the mesoporous TiO_2 layer, we used a 30 N-RD TiO_2 paste (Dyesol) diluted to approximately 150 mg per millilitre of ethanol. After vigorous stirring (30 min), it was spin coated on the TiO_2 compact layer (4000 rpm, 20 s) and then annealed at 450 °C for 1 h.

For the preparing of ZnO-TiO_2 bilayer as ETL, first the ZnO NR were prepared as described above. TiO_2 solution was prepared as described above for the compact TiO_2 layer and spin coated (100 µL at 3000 rpm for 30 s, dried at 150 °C for 15 min) on the ZnO NR substrates. Prepared TiO_2 coated ZnO NR substrates were washed using MiliQ water and dried in nitrogen stream and thermally treated at 400 °C for 1 h in tube furnace.

For the deposition of photoactive perovskites, the following 1.5 M solutions were prepared in 4:1 V/V DMF (dimethylformamide) / DMSO (dimethyl sulfoxide): (1) $PbBr_2$ (lead bromide, p.a. Sigma Aldrich, Netherlands), (2) PbI_2 (lead iodide, p.a. Sigma Aldrich, Netherlands), (3) CsI (caesium iodide, p.a. Sigma Aldrich, Netherlands) (just DMSO), (4) RbI (rubidium iodide, p.a. Sigma Aldrich, Netherlands). Normally, the prepared solutions were heated on a hot plate to 180 °C until complete dissolution. Thereafter, FAI (formamidinium iodide, CNH_2NH IH, p.a. Sigma Aldrich, Netherlands) was dissolved at RT in solution 1) with 9 % lead excess, and MAI (methylammonium iodide, CH_3NH_2 IH, p.a. Sigma Aldrich, Netherlands) was dissolved at RT in solution 2 with 9 % lead excess. Combination of the above solutions (1) and (2) yield MA-FA solution which was heated on a hot plate heated to 150 °C until complete dissolution. To increase the stability, the MAFA solution was combined with solutions (3) and (4), to yield Cs-Rb-MA-FA solution. The stoichiometry was followed according to the quadruple cation perovskite formula $(MA_5FA_1)_{0.9}(Rb_3Cs_3)_{0.1}$ Pb_6 $(I_5Br_1)_3$. The hole transporting layer (HTL) was prepared by mixing spiro-OMeTAD (N^2,N^2,$N^{2'}$,$N^{2'}$,N^7,N^7,$N^{7'}$,$N^{7'}$-octakis(4-methoxyphenyl)-9,9′-spirobi[9H-fluoren]-2,2′,7,7′-tetramin, $C_{81}H_{68}N_4O_8$, p.a. Sigma Aldrich, Netherlands) with LiTFSI (bis(trifluoromethane) sulfonimide lithium salt, $CF_3SO_2NLiSO_2CF_3$, p.a. Sigma Aldrich, Netherlands) and FK209 (tris(2-(1H-pyrazol-1-yl)-4-tert-butylpyridine) cobalt(III) tri [bis(trifluoromethane) sulfonimide], $C_{42}H_{45}CoF_{18}O_{12}N_{12}S_6$, p.a. Sigma Aldrich, Netherlands).

Electrode material (gold) was used as received.

2.2. PSC Assembly

Glass/ITO was used (ITO 200 nm) was used as a substrate. For the adjacent ETL, three variations were used: (1) Zincite vertical ordered nanorods (less than 400 nm; prepared as described above; deposited by a 2 step spin coating of the seed layer and chemical bath growth reaction of the ordered nanorods). (2) Anatase mesoporous layer (around 600 nm; prepared as described above; deposited by spin coating a planar layer and then a mesoporous layer, thermally treated). (3) Zincite vertical ordered nanorods additionally coated by titania (ZnO NR less than 400 nm; prepared as described above; deposited by a 2 step spin coating of the seed layer and chemical bath growth reaction of the ordered nanorods. TiO_2 less than 35 nm; sol-gel solution prepared as described above; deposited by spin coating). Subsequently, the quadruple cation photoactive perovskite material was deposited ($(MA_5FA_1)_{0.9}(Rb_3Cs_3)_{0.1}$ Pb_6 $(I_5Br_1)_3$) with an additional antisolvent step in the last 10 s of the spin coating (75 µl of chlorobenzene) (800 nm). Spiro-OMeTAD was deposited by spin coating (~100 nm, additives: LiTFSI and FK209). Gold was deposited by thermal evaporation (100 nm). Depending on the type of the ETL, the prepared samples were zincite nanorods closed solar cell (ZnO-PSC), mesostructured titania closed solar cell (TiO_2-PSC), and a combination closed solar cell (ZnO-TiO_2-PSC) (**Table 1**).

2.3. Characterisation

In-situ characterization was performed using synchrotron radiation at the MCX beamline of the Elettra Synchrotron facility in Trieste using a self-developed multifunctional in-situ cell for simultaneous GIXRD/XRR/Raman characterizations as a function of temperature on multi-layered thin films. Inside of a Huber 4-axis goniometer, a resistor-heated (3 serial CQC6R8J 9 W resistors), air convection-cooled aluminium hotplate (hollow Al 8×6×2 cm box, resistors glued by silicone thermo-glue inside in ceiling position, insulator wool at bottom) was mounted on a stage, 5 mm thick Teflon disc was used to insulate hotplate from stage. The heating cell was regulated by HWE 12 V DC thermistor-based controller. A multichannel Siglent SPD3303S power supply device ensured 12 V DC to a thermistor temperature controller and fixed 14 V DC (21 W) to resistor series that served as a heating source. The exact temperature was corrected by K-type thermocouples via a multichannel Pico TC-08 data logger. Planar samples were positioned flat on the hotplate surface. The hotplate stage was adjusted in plane using z-scan and θ-scan. Measurements were performed isothermally, for RT measurements the temperature was maintained at 25°C. Measurements were performed in ambient air; relative humidity was maintained at 20 %. Raman optical sensor was mounted vertical to the hotplate stage and focused at 7 mm distance. The Raman sensor was connected to the stage so the beam remained in focus during GIXRD geometry adjustments. Samples were excited using a PD-LD LS-2 100 mW laser at a wavelength of 635 nm. Scans were collected using Maya2000Pro Ocean Optics device in 100–1200 s^{-1} range with 10 s collecting time. Additional Raman spectroscopy measurements were preformed using a HORIBA Jobin Yvon T64000 spectrometer with a 532.5 nm solid-state laser excitation in micro-Raman mode. Laser power of 20 mW at the sample, and an objective with a 50× magnification (Olympus) were used. Grazing incidence diffraction analysis (GID) was performed using a monochromatic 8 keV beam (spot size 300×1000 µm) at several incidence angles (0.40, 0.75, 1.50) in a 2θ range of 15–45°, with continuous steps 0.01°2θ and collecting time of 0.2 s (slits 0.4; 0.3 µm).

Current-voltage (IV) curves were recorded in a glovebox using a Keithley 2400 source measure unit and a custom made LabView software. The samples were illuminated by a Dedolight DLH400 lamp with a spectrum similar to the AM 1.5 G spectrum at 100 mW cm^{-2}.

FTIR spectroscopy was performed using a Bruker Vertex 70 in ATR (attenuated total reflectance) mode. The samples were pressed on a diamond and the absorbance data were collected between 400 and 4000 cm^{-1} with spectral resolution of 1 cm^{-1} and 64 scans.

The field emission scanning electron microscopy (FESEM) images were taken with a JEOL thermal field emission scanning electron microscope (model JSM-7000F). The FESEM was coupled with an energy dispersive X-ray analyser (EDS) (Oxford Instruments EDS/INCA 350).

Atomic force microscopy (AFM) images were taken using a Nanosurf CoreAFM under ambient conditions. Non-contact (tapping) mode was used for acquisition with a setpoint in the range from 30 to 50 % with Tap300Al-G tip with a nominal spring constant of 40 N m^{-1}, a tip radius less than 10 nm and a nominal resonant frequency of 300 kHz on a 2×2 μm surface with 0.78 s acquisition time. Images were processed with Nanosurf software.

The focused ion beam (FIB) derived lamella and SEM images were prepared using a FEI Helios Nanolab 650. Prior to the FIB lamella preparation, a Pt layer was deposited as protection layer. All the scanning transmission electron microscopy (STEM) imaging and spectroscopy was performed using a dedicated TEM equipped with a 4 quadrant Super X detector for EDS. Every layer's thickness was measured 5 times along the FIB cross sections/FIB lamellas.

2.4. Description of degradations tests

The PSCs (**Table 1**) were prepared and sealed in protective atmosphere. The PSC samples were exposed to ambient conditions (20 % humidity) for mounting purpose 5 min before in-situ GID/Raman f(T) experiment. First spectra were collected at RT and 20 % relative humidity – normal degradation. The collection of the data took one hour. GID/Raman f(T) measurements were repeated at RT, which took another hour. Thereafter at least 4 GID/Raman f(T) measurements were performed at elevated temperature (isothermally at 50 °C) (additional 4+ hours). Another GID/Raman f(T) set of measurements was collected at RT scan after one hour of cooling. These scan sets represent enhanced degradation. In addition, we conducted additionally enhanced degradation for selected samples, where the degradation was performed at 90 °C instead of 50 °C.

Measurements to determine IV characteristics, SEM/EDS, FIB/STEM, Raman were performed in protective atmosphere or after in-situ tests on open/closed PSC cells or immediately upon exposure to ambient conditions on cloned PSC samples. Measurements to collect FTIR, AMF were performed on open/closed PSC cells exposed to ambient conditions for one month (open cells: without top layer (Au electrode); closed cells: with top layer (Au electrode)).

Table 1. *PSC sample degradation conditions and denomination.*

Sample / incidence angle	**Conditions**						
	RT (0–1h)	**RT (1–2h)**	**50 °C* (2–3h)**	**50 °C* (3–4h)**	**50 °C* (4–5h)**	**50 °C* (5–6h)**	**RT (7–8h)**
(A) series: ZnO-PSC	**Datasets**						
0.40°θ	Z0_040	Z1_040	Z2_040	Z3_040	Z4_040	Z5_040	Z6_040
0.75°θ	Z0_075	Z1_075	Z2_075	Z3_075	Z4_075	Z5_075	Z6_075
1.50°θ	Z0_150	Z1_150	Z2_150	Z3_150	Z4_150	Z5_150	Z6_150
(B) series: TiO_2-PSC	**Datasets**						
0.40°θ	T0_040	T1_040	T2_040	T3_040	T4_040	T5_040	T6_040
0.75°θ	T0_075	T1_075	T2_075	T3_075	T4_075	T5_075	T6_075
1.50°θ	T0_150	T1_150	T2_150	T3_150	T4_150	T5_150	T6_150
(C) series: ZnO-TiO_2-PSC	**Datasets**						
0.40°θ	T0_040	T1_040	T2_040	T3_040	T4_040	T5_040	T6_040
0.75°θ	T0_075	T1_075	T2_075	T3_075	T4_075	T5_075	T6_075
1.50°θ	T0_150	T1_150	T2_150	T3_150	T4_150	T5_150	T6_150

*samples NR ZnO open solar cells were degraded at 90 °C.

3. Results and Discussion

3.1. System selection and experiment planning

Initially the closed cells (with gold electrodes) were tested regarding their photovoltaic performance and their PCE values are in concordance with reported values for similar types of PSCs. Not so long ago, all PSCs showed rapid degradation of PCE values after exposure to moisture in air; i.e., PSCs demonstrated extreme sensitivity to atmospheric conditions. Applying considerable protection was a partial solution, since the source of the degradation could arise from external (ambient air moisture), but also from internal (already the deviation from proper protective atmospheric conditions of <0.1 ppm of O_2 and H_2O will cause discrepancies in the course of the synthesis and assembly). Modern PSCs do not show extreme moisture sensitivity. The PSC system selected for this investigation is an example of the modern PSC comprising all recent modifications that have been reported to favour the increase in stability, i.e., resistance against degradation in atmospheric conditions. We monitored primarily the structural but also microstructural surface and chemical origin of the degradation. Electrical performance came secondary. Namely, for enhanced in-situ testing, we chose open cells. Therefore, closing of the cells after the degradation experiment for the IV and PCE tests would not yield comparable results, and thus was omitted. From the configuration point of

view, for the n-i-p type of device, commonly known as normal PSC (**Figure 1**), we encountered five main constituting layers in order of assembly:

(i) Transparent conducting oxide layer (TCL) was, in this case, ITO on a glass substrate. This layer is known to be mechanically durable and chemically stable, and can hardly be a parameter in the course of the PSC degradation. However, other layers are deposited on top of this layer, so any irregularity in the initial layer enhances subsequent problems. That is particularly evident for the case of the nanostructured subsequent layers.

(ii) The electron transfer oxide layer (ETL) is also not especially prone to degradation, although the ETL plays a critical role in modern PSCs. Namely, the capability of the perovskite layer to absorb a lot of light cannot be utilised unless the generated excitons are not separated and charge carriers transferred to the electrodes. Beside chemically favourable compositions of the ETLs, here critically important are the morphology, geometry, and surface conditions. Namely, this is the layer adjacent to perovskite absorber, so any interfacing incompatibility would certainly directly diminish the overall PSC performance indicators. Trying out various nanostructured ETLs, such as titania nanotubes, or zincite nanorods, is well worth the risk, since the expected benefits reflect in strong enhancement of the charge carrier transport on behalf of increased number of charge transport pathways due to higher specific surface, as well as more vectorised charge transport pathways due to 1D or 2D geometry. However, the following layers show much stronger susceptibility for humidity-induced degradation, making the ETL comparison difficult. The idea of this work was to interchange between conventional ETLs in advanced configuration:
   - **(A) Series:** Zincite nanorods. Zincite is probably the most abundant ETL, where nanorod configuration utilises enhanced specific surface and increased 1D order to vectorise performance.
   - **(B) Series:** Mesoporous anatase. Anatase is perhaps the most widespread ETL, but in mesoporous configuration, it utilises enhanced specific surface, which further increases performance.
   - **(C) Series:** Combination of titania on zincite nanorods. These ETLs will allow discussion on derivative causes, consequences, and manifestation of degradation. The aim was to extrapolate the observation of degradation consequences to a whole cell, and to observe degradation repercussions on layers other than the perovskite and spiro-OMeTAD.

(iii) The photoactive layer in PSCs is commonly a hybrid perovskite, such as $MAPbI_3$ or $(MA,FA)PbI_3$. The degradation of this layer is affected primarily by humidity. Besides introducing layers that hinder the diffusion of the moisture towards perovskite layers in the closed cells, advances in the synthesis stage have been made to make the precursor solutions less prone to hydrolysis [**7**]. Perovskite precursor solutions based on multiple cations are currently considered the most stable against moisture. We used Cs-Rb-MA-FA ($(MA_5FA_1)_{0.9}(Rb_3Cs_3)_{0.1}Pb_6(I_5Br_1)_3$). We kept to the composition that was proven as the most stable in our group.

(iv) Hole transport layers (HLT) for perovskite systems need to be quite specific, and such layers are again prone to hydrolysis. Nanostructuring of the layers is still infeasible, but additives that increase stability and performance have been identified **[38]**. We used spiro-OMeTAD with LiTFSI and FK209. We again kept to the composition that was proven as the most stable in our group. The interface perovskite-HTL is the most heavily affected in the PSC degradation, but this interface has also been heavily explored.

(v) Top electrode is a gold thin-film. In contrast to the general opinion that gold will be inert and hinder water diffusion, that is rarely the case.

The course toward degradation and the samples were selected to answer two main questions. The first being the influence of the different commonly used ETL layers; **(A) series:** zincite nanorods, **(B) series:** mesoporous titania, and **(C) series:** their combination, on the course of the degradation. The second question was the susceptibility of the PSC to moisture as a function of temperature. Namely, PSCs are definitively prone to hydrolysis in humid conditions. Only thermally induced degradation is well documented. However, the pathway of thermal degradation in humid conditions is not perfectly clear. The discrepancies arise from the fact that, sometimes, application of a thermal regime may be beneficial for the system exposed to humid conditions; in other cases, it can be additionally detrimental. The question is whether a thermal regime can supress the inter-diffusion of the humidity, and consequently, the damage. Therefore, we planned an in-situ synchrotron radiation GID-Raman experiment to monitor the structural (and to a certain extent chemical) degradation of the entire PSC devices. Outside the scope of the in-situ experiment, characterisation was broadened to include FTIR, AFM, and SEM/EDS to reveal additional compositional, surface, and chemical conditions after the simulated degradation. In addition, selected samples were subjected to FIB to prepare representative cross-sections for the STEM analysis.

The J/V measurements were performed discretely upon assembly in protective atmosphere. Current voltage characteristics of selected assembled devices are shown in **Figure 2**, while the parameters of the best solar cells are highlighted in **Table 2**. For the case of (A) and (B) configurations, the solar cells revealed a hysteresis, which is typical for all PSCs, with quite large hysteresis indexes, indicating unbalanced electron/hole transport due to charge carrier accumulation at interfaces. Devices assembled with ZnO ETLs did not reveal photovoltages and fill factors as high as devices containing TiO_2 ETLs, which may already indicate a less-than-perfect ETL/absorber interface. Namely, any inconsistency in ZnO-nanorod surface and orientation homogeneity, as well as generally increased ETL surface roughness, and uneven lengths of the rods on the entire surface of the cell, can lead to an increased number of defects at the perovskite/ZnO interface, i.e., lower fill factor and greater series resistance of ZnO devices in comparison to TiO_2. At this point, it was unclear how this would affect degradation stability.

To test the stability of the perovskite on the MS TiO_2-based ETL, the initial perovskite solution was diluted 10×. Interestingly, these PSCs showed a slightly better PCE pointing out that this concentration also leads to sufficiently high absorber layer thicknesses. **[39]**.

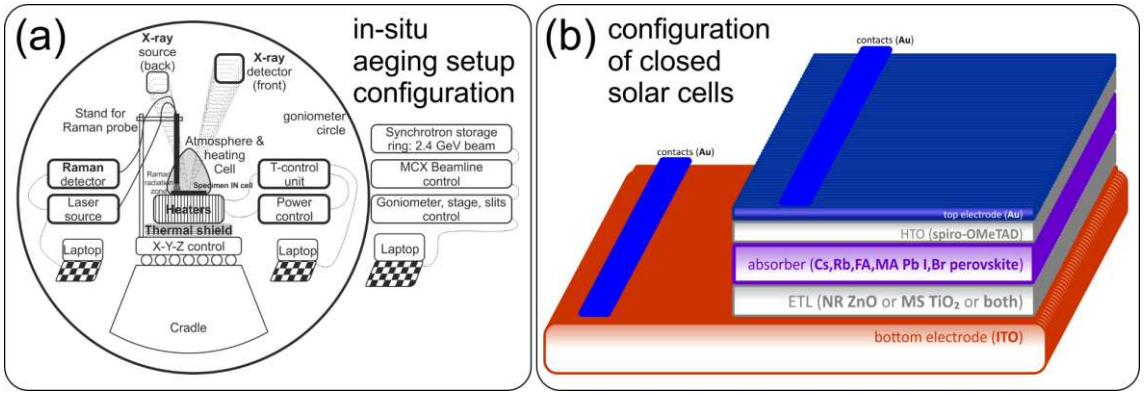

Figure 1. ***(a)*** *Scheme of the in-situ setup, and* ***(b)*** *Geometry of the n-i-p configuration of the solar cells comprising the NR ZnO, MS TiO_2, or ZnO-TiO_2 ETLs.*

Table 2. *J/V characteristic of selected ZnO and TiO_2 closed solar cells.*

Sample	V_{OC} / V	J_{SC} / $mAcm^{-2}$	FF / %	PCE / %	R_S / Ωcm^2	R_{shunt} / Ωcm^2	HI / %
NR ZnO-PSC	0.95	19.63	62.7	11.5	31.00	176	45.2
MS TiO_2-PSC	0.99	20.36	71.5	14.5	4.35	161	45.9
MS TiO_2-diluted-PSC*	1.00	22.29	67.7	15.1	4.40	157	57.0

*dilution during the synthesis explained in the text

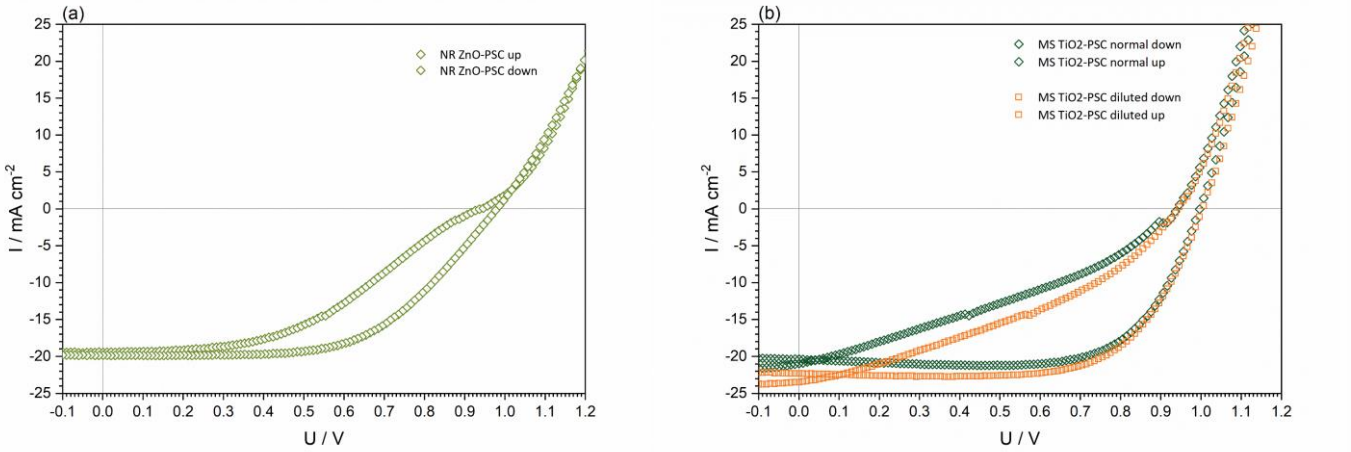

Figure 2. *Summary of IV characteristics measurements for selected open cells;* ***(a)*** *NR ZnO-closed solar cell, and* ***(b)*** *MS TiO_2-closed solar cell, and MS TiO_2-diluted-closed solar cell.*

3.2. In-situ degradation of PSCs (at ambient conditions and at levels of thermally enhanced conditions)

Crystalline composition observed from X-ray grazing incidence diffraction analysis was the main parameter for assessment of stability. Namely, since we chose to work with open/closed operative cells (no top electrode for open cells), they were prone to gradual degradation under air atmosphere. The diffusion of air, moisture, and oxygen into the absorber, having in mind that perovskites readily oxidise, is the main limiting factor to the widespread use of PSC systems. Photoactive perovskites decompose into constituent salts, such as PbI_2, etc. Monitoring the presence of crystalline perovskite phases and decomposition product phases is the key to evaluating stability and decomposition dynamics. When analysing solely the hybrid perovskite layer without being covered by an additional layer, the degradation is so fast that even immediately after fabrication, i.e., upon removal of samples from the protective atmosphere, the degradation takes place and prevents collecting a reference scan of the pristine non-degraded perovskite layer. However, for closed perovskite solar cells, the degradation is not so fast, and a reference scan can be collected. Nevertheless, in closed cells, perovskite precursor salts (such as lead iodide) are commonly present in excess to increase conductivity. To differentiate initial quantity of precursor salts and decomposition products, we used other features of the PSC. Namely, other layers, such as transparent electrodes (commercial ITO substrates) and conventional electrodes (gold deposited via thermal evaporation) give rise to a reproducible diffraction signal. Since the PSCs (especially electrodes) are geometrically equivalent, and the positioning in the XRD holder is the same, the diffraction patterns of the electrodes can be used to quantify initially present precursor salts on behalf of relative intensity ratios during the temperature treatment. In addition, the kinetics of the decomposition can be monitored. The analysis was performed as discussed above in the experimental sections and the data are shown in **Figure 3 and 4**.

(i) Glass substrates are amorphous. Even the main peaks of ITO, according to indium oxide (ICDD PDF#06-0416), were not visible for all samples. Despite the fact that ITO normally displays a strong XRD signal, having in mind the PSC configuration where the ITO was at the bottom of the SC, the absence of the signal is quite normal.

(2) Superstructural peaks originating from **zincite nanorods** or **mesostructured titania** could not be detected due to low intensity. However, a mesostructural peak was observed at 1.87 °2θ, resembling a 4.7 nm phenomena. The main peak of anatase was barely visible (presence in traces) according to ICDD PDF#21-1272 in all PSCs having titania-based ETL; (B) and (C) series. In all PSCs having zincite nanorods for ETL, the main zincite peaks could be barely observed according to ICDD PDF#36-1451; (A) and (C) series. Such a low zincite signal may suggest better coverage of zincite layer with adjacent perovskite layer than in the case of titania, but it may also indicate poor development of the layer. The mesoporous titania films (despite similar thicknesses of both ETL layers) only partially allowed infiltration of the perovskite precursors, whereas the perovskite precursors could engulf the ordered exposed zincite nanorods much more easily and in larger quantity, consequently reducing the zincite XRD signal. In the case of poor formation of the zincite, the signal would also be affected.

(iii) Main hybrid perovskite peaks were visible at about 14 °2θ and shifting slightly in 2θ, depending on the cations used in the perovskite configuration. Peaks stemming from the perovskite and decomposition products were used for monitoring of process of the PSC degradation.

For the titania open cell (**Figure 3c**), the perovskite peak intensity decreased with thermal aging, suggesting gradual degradation of the perovskite phase. Despite the fact that realignment was conducted at each temperature, the thermal expansion of the stage could have also slightly reduced the XRD signal. With thermal aging, the perovskite peaks shifted slightly, suggesting the unit cell might have been affected.

For the zincite open cell (**Figure 3a**), the signal was much more diffuse and lower in intensity, suggesting less order. With thermal aging, the peaks generally did not shift, which suggested the unit cell had not really been affected. Interestingly, with aging, and in contrary to titania open cell behaviour, peaks decreased intensity much more gradually. This could indicate thermally induced (micro)structural relaxation. Namely, it might simply be assumed that the initial organisation of the interface was probably not really obtained, so that the thermal aging actually served as a facilitator for somewhat better ordering before triggering degradation.

For the case of the zincite-titania open cell (**Figure 3e**), the predominant behaviour was similar to titania open cell in almost all aspects. The effect of depth profiling can here be illustrated by the relative intensity ratio (RIR) of the peaks characteristic for the perovskite phase and perovskite decomposition products. Apparently, the RIR differed with depth, which can be related to greater exposure of the upper part of the open cell to ambient humidity in comparison to the lower part.

For all closed cells (**Figure 3b,d,f**), the thermal degradation showed a decrease in the intensities, with no shifting of peaks or other unexpected phenomena.

The changes of the main peaks of **perovskite precursor but also the decomposition product** PbI_2 (according to ICDD PDF#07-0235), (and other such as $PbBr_2$, NH_4I, NH_4Br, etc), point to the decomposition process. Moreover, a perovskite photo-inactive co-product, the hexagonal d-phase (yellow perovskite) of $FAIPbI_3$, was present at 11.6 °2θ. This is a very typical observation for the mixed perovskite composition showing incomplete conversion of the FA perovskite into the photoactive black phase. Upon addition of small amounts of Cs, the yellow phase and the PbI_2 peak may disappear, however, they reappear over degradation. The data is consistent with the Rb and Cs cations being integrated into the perovskite lattice. Smaller Cs and Rb, when combined with MA/FA, consequently lower the effective Cs/Rb/MA/FA cation radius in the new perovskite compound. This shifts the tolerance factor towards a cubic lattice structure that matches the black perovskite phase, which entropically stabilises the photoactive black phase at room temperature, suppressing the hexagonal yellow phase of FA perovskite. Interestingly, phase separation may appear at higher doping concentrations, due to a large size mismatch between two cations, such as Cs and FA **[39]**. However, the use of a triple cation mixture minimised this constraint, as the relative differences in sizes of the cations were smaller. This in turn decreased the entropic preference for phase separation and again supressed yellow perovskite appearance.

(iv) spiro-OMeTAD and FK209 additives are predominately amorphous; however, the LiTFSI additive showed crystalline peaks at 15 and 20 °2θ, but generally, such weak patterns cannot be clearly resolved using Bragg-Brentano XRD setup.

(v) Main **Au** peaks point to major presence (according to ICDD PDF#04-0784).

For the case of proven stability at ambient and thermally enhanced degradation, for pragmatic reasons, only one selected cell (NR ZnO-closed solar cell) was subjected to additionally thermally enhanced degradation (90 °C instead of 50 °C), where, unquestionably, the presence of degradation by-products was evident. For the selected cell, the additionally enhanced aging (thermal degradation) yielded a more pronounced decrease in the XRD signal. Shortly, from the absorber point of view, one can say that 4-cation composition generally proved viable for the case where ambient stability was required. The perovskite absorbers also proved viable for the case of enhanced degradation. However, even advanced composition PSC absorbers have limits, which the additionally enhanced degradation proved. Our intention was not to focus solely on the absorber, but to compile the contributions from the interfaces of absorber and inorganic nanostructured ETLs.

However, from the point of view of ETL, compiling of the degradation contributions is much more complex. Namely, the ETL layer does not undergo bulk degradation, as does the absorber layer, so from the characterisation point of view, it is much more difficult to observe and pinpoint the degradation of the ETL layer. However, a very good assumption can be made that the degradation is caused, or at least enhanced, at the ETL/absorber interface, which was already indicated from the initial IV and PCE properties. The complex interface between the nanostructured inorganic ETL and the 4-cation absorber was well "hidden" and proved outside the scope of our in-situ characterisation setup, despite its elaborated configuration. Therefore, we had to subject samples to a few additional characterisations.

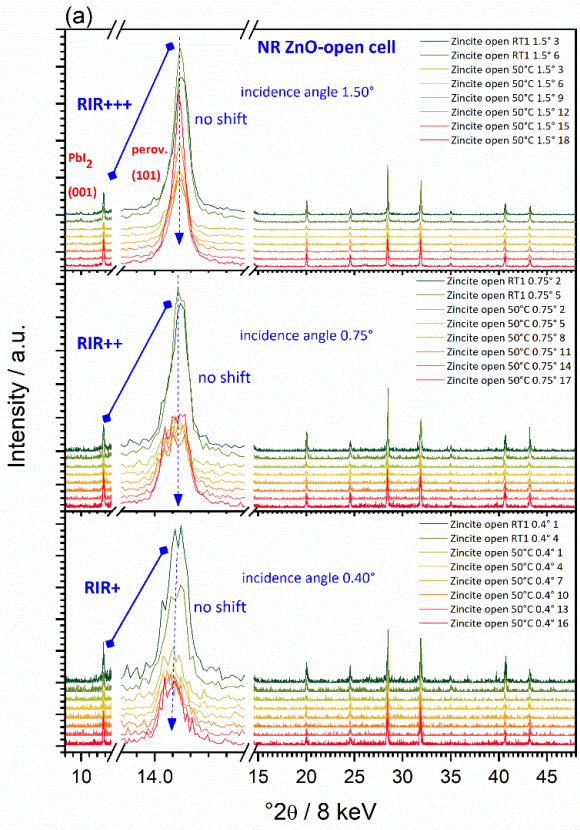
(a)
NR ZnO-open cell
RIR+++
RIR++
RIR+
PbI2
(001)
perov.
(101)
incidence angle 1.50°
incidence angle 0.75°
incidence angle 0.40°
no shift
Intensity / a.u.
°2θ / 8 keV

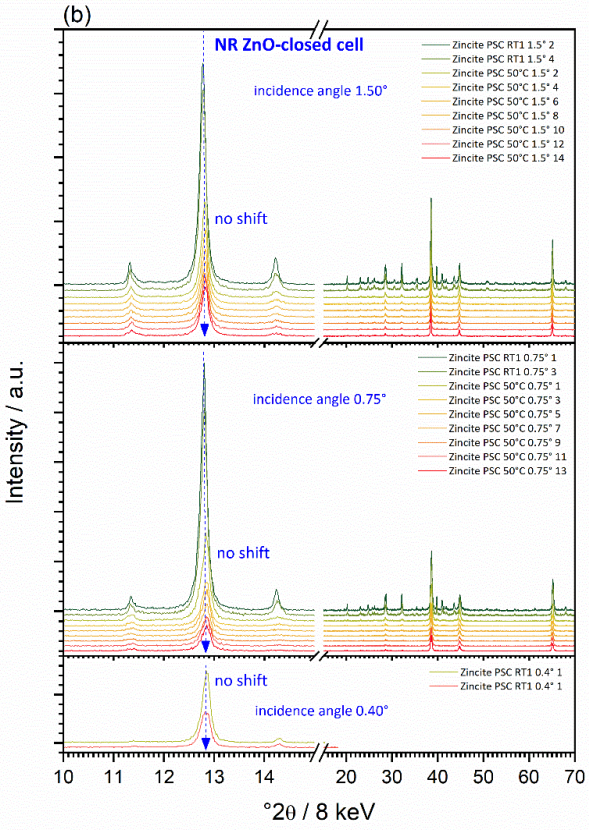
(b)
NR ZnO-closed cell
incidence angle 1.50°
incidence angle 0.75°
incidence angle 0.40°
no shift
Intensity / a.u.
°2θ / 8 keV

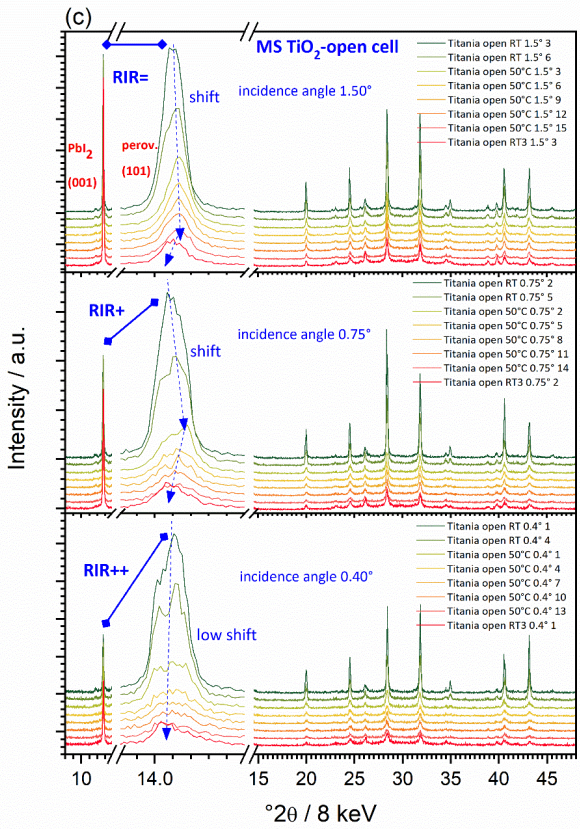
(c)
MS TiO2-open cell
RIR=
RIR+
RIR++
PbI2
(001)
perov.
(101)
shift
low shift
incidence angle 1.50°
incidence angle 0.75°
incidence angle 0.40°
Intensity / a.u.
°2θ / 8 keV

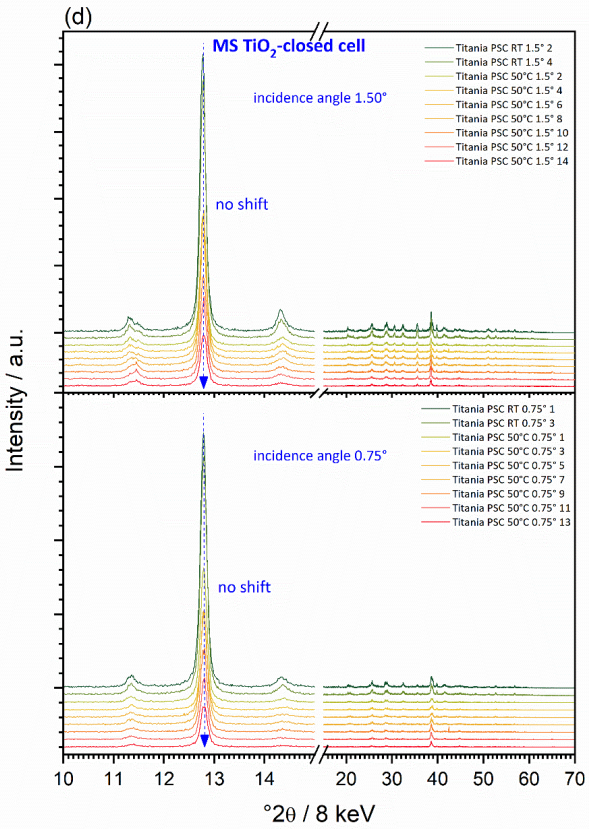
(d)
MS TiO2-closed cell
incidence angle 1.50°
incidence angle 0.75°
no shift
Intensity / a.u.
°2θ / 8 keV

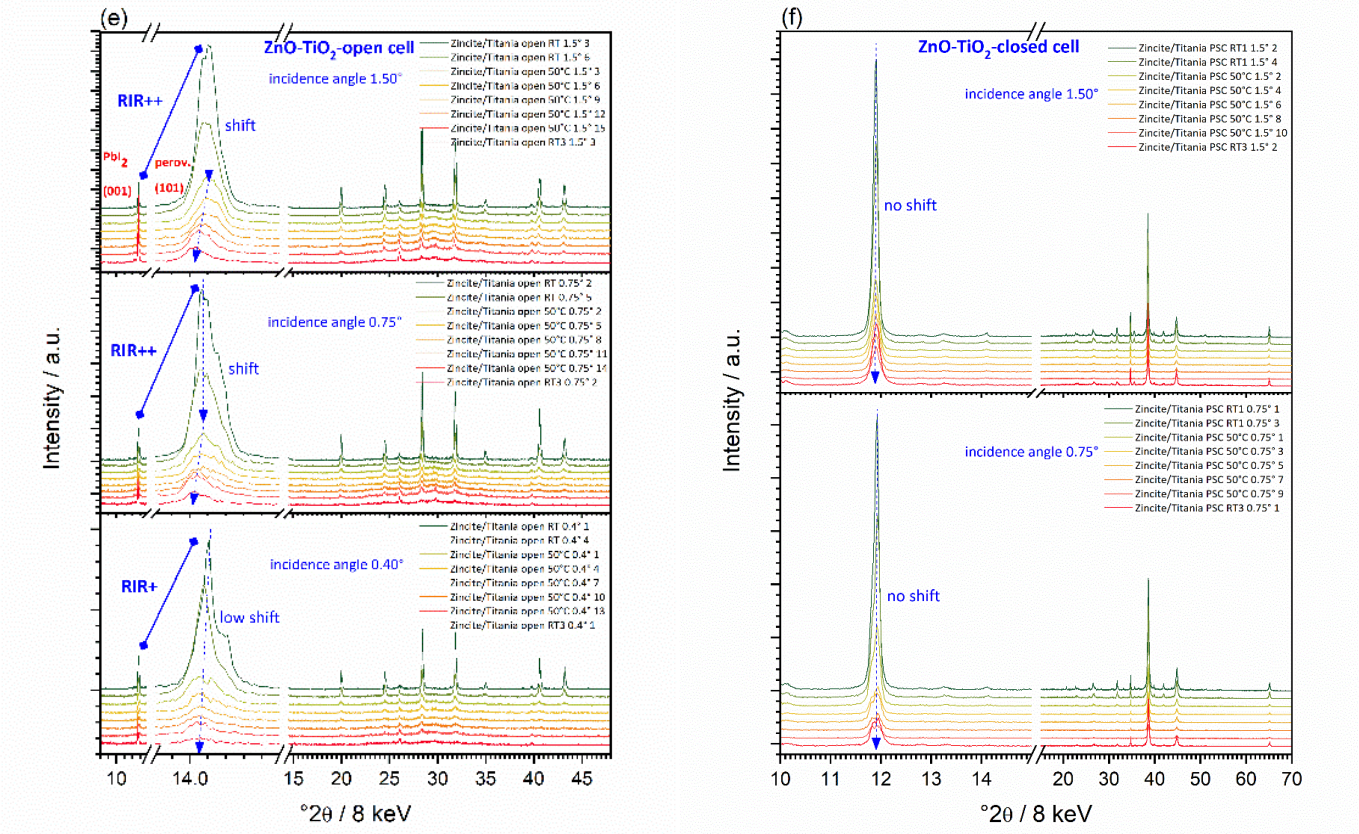

Figure 3. *In-situ RT degradation and thermally enhanced degradation, including RT relaxation: GID depth profiling at several incidence angles of the solar cell samples;* ***(a)*** *ZnO-based open solar cell;* ***(b)*** *ZnO-based closed solar cell;* ***(c)*** *TiO_2-based open solar cell;* ***(d)*** *TiO_2-based closed solar cell;* ***(e)*** *ZnO-TiO_2-based open solar cell;* ***(f)*** *ZnO-TiO_2-based closed solar cell.*

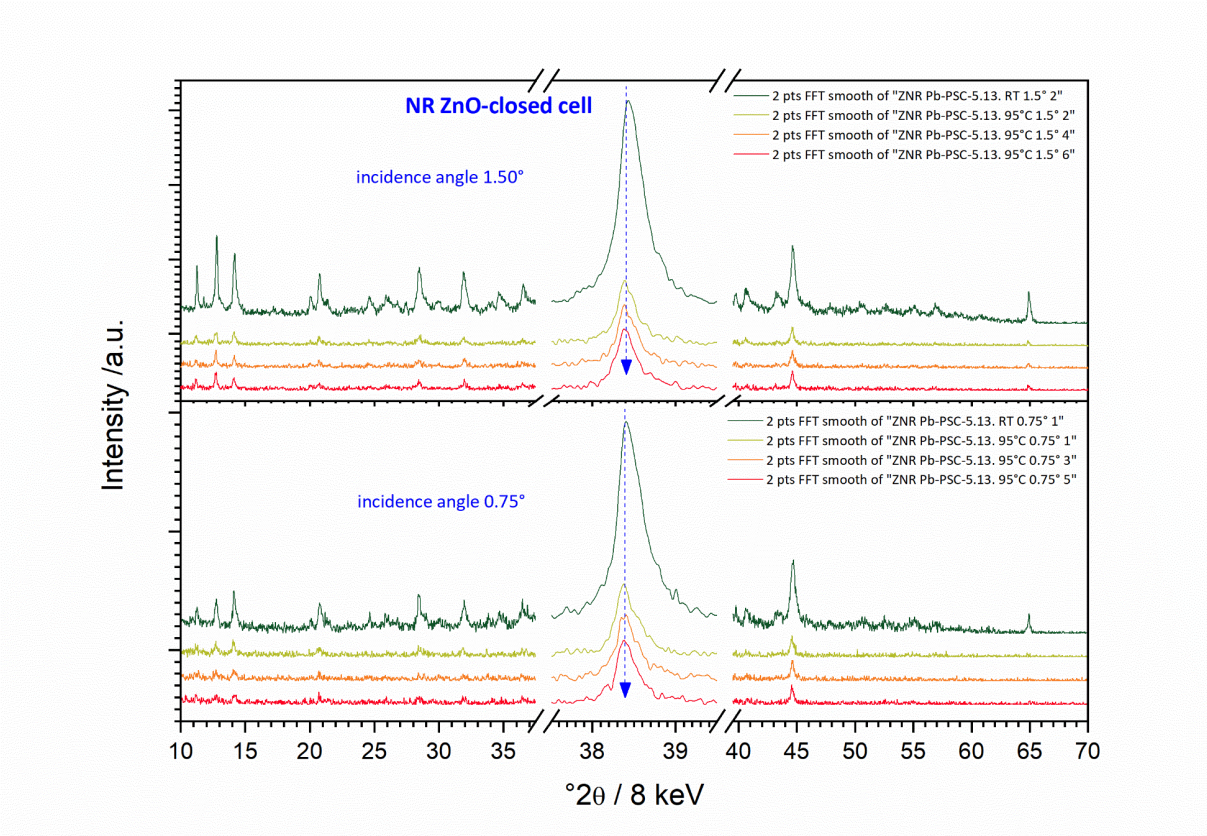

Figure 4. *Additionally, thermally enhanced degradation for closed NR ZnO-closed solar cell: GID depth profiling at several incidence angles of cells.*

3.3. General characterisation of PSCs outside the scope of in-situ experiment

For the case of characterisation outside the scope of in-situ experiment, by looking into functional vs. structural vs. aging perspective of the perovskite solar cells we revealed performance vs. stability parameters. Because solar cells were assembled, the performed analyses are only partially informative, since considerable useful information can be shielded by surface layers. FTIR spectroscopy gave additional information about the perovskite. As seen in **Figure 5a,** the differences arose only from the different ETL used. The TiO_2-based solar cells showed additional bands at around 3200 cm^{-1} from N-H stretch **[40],** which indicated that those samples could have degraded further than the samples with ZnO NR, which aligns with the whole discussion leading to this point that ZnO-based devices can be more stable **[10].** Bands characteristic of the substrate (glass, at around 1000 cm^{-1}) were present for all samples.

The Raman spectroscopy measurements suggested that most of the signals originated from the organic molecules (several candidates) **[41],** but the lead halides were not detected in this range. Since the signals originating from the halides are found below 250 cm^{-1}, and were beyond the scope of the instrument setup, the Raman data could not shed more details on the degradation process, unfortunately. Hence, only PSCs based on mesoporous titania are shown as an example in **Figure 5b**.

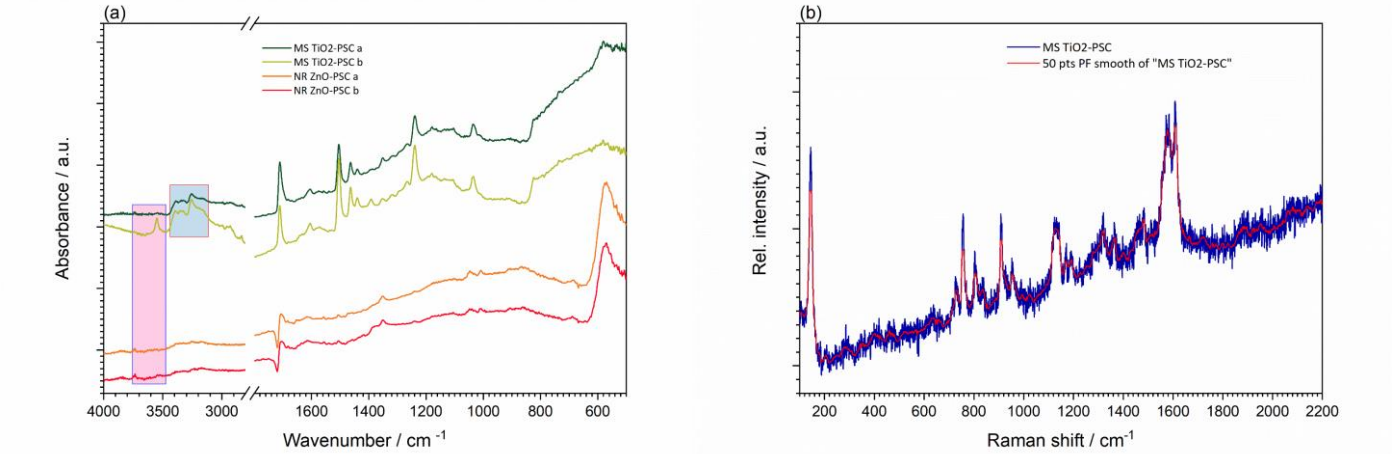

Figure 5. *Summary of measurements for selected open/closed cells; NR ZnO, MS TiO_2 (pink and blue shaded areas show peak for N-H bonds);* ***(a)*** *ATR-FTIR;* ***(b)*** *micro-Raman spectroscopy.*

SEM EDS measurements revealed information about the morphology and the composition. Already at first sight, one can observe that the perovskite layer had formed better on TiO_2 ETL than on ZnO in terms of grain growth, grain and pore size and distribution, so derivatively, adhesion and homogeneity. This can be better observed from cross-sections (**Figure 6a**). EDS analysis also showed more homogeneous distributions of all elements, as expected for the case of MS TiO_2-closed solar cell (**Figure 8c,f**). However, the aspect of the infiltration of the perovskite layer into the nanorods throughout the depth was confirmed. Yet, these results are far from conclusive in terms of system electrical performance, and particularly in terms of understanding the degradation.

AFM results corroborate well with the FESEM characterization. From the topography and phase scan, we can further observe discrepancies in the perovskite layer formation on the MS TiO_2 ETL (**Figure 7a**), in comparison to the NR ZnO ETL (**Figure 7b**); they are even more obvious from the 3D representations of the scans. The surface roughness values of 10.2 nm and 26.0 nm for ZnO and TiO_2, respectively, indicate small non-agglomerated perovskite grain formations, but since the sample with ZnO had many voids and the *Sq* value gives a statistically average value of the whole surface (2×2 μm) the low values for ZnO have to be taken with caution since they maybe me misleading.

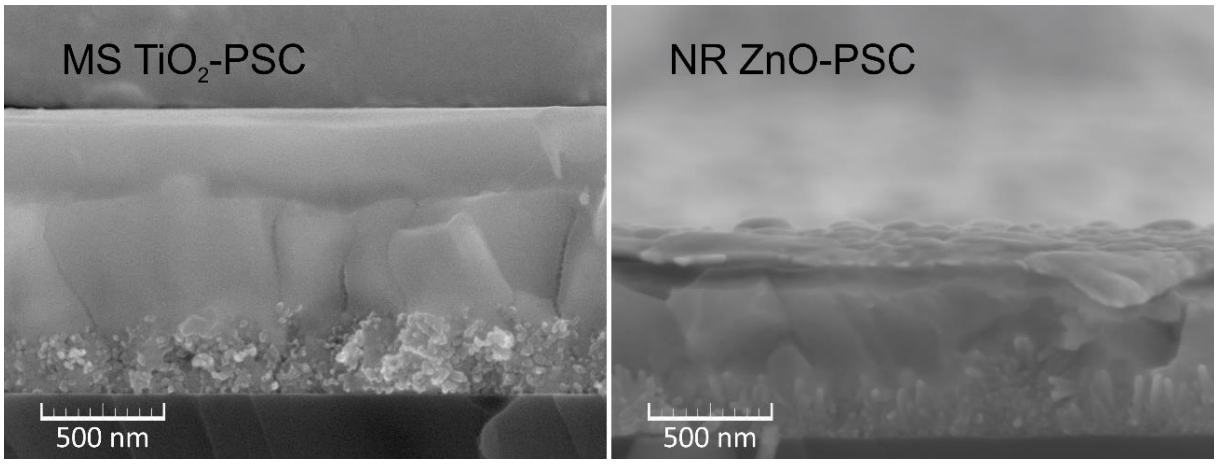

Figure 6*. FESEM micrographs of selected;* ***(a)*** *MS TiO_2-closed solar cell;* ***(b)*** *NR ZnO-closed solar cell.*

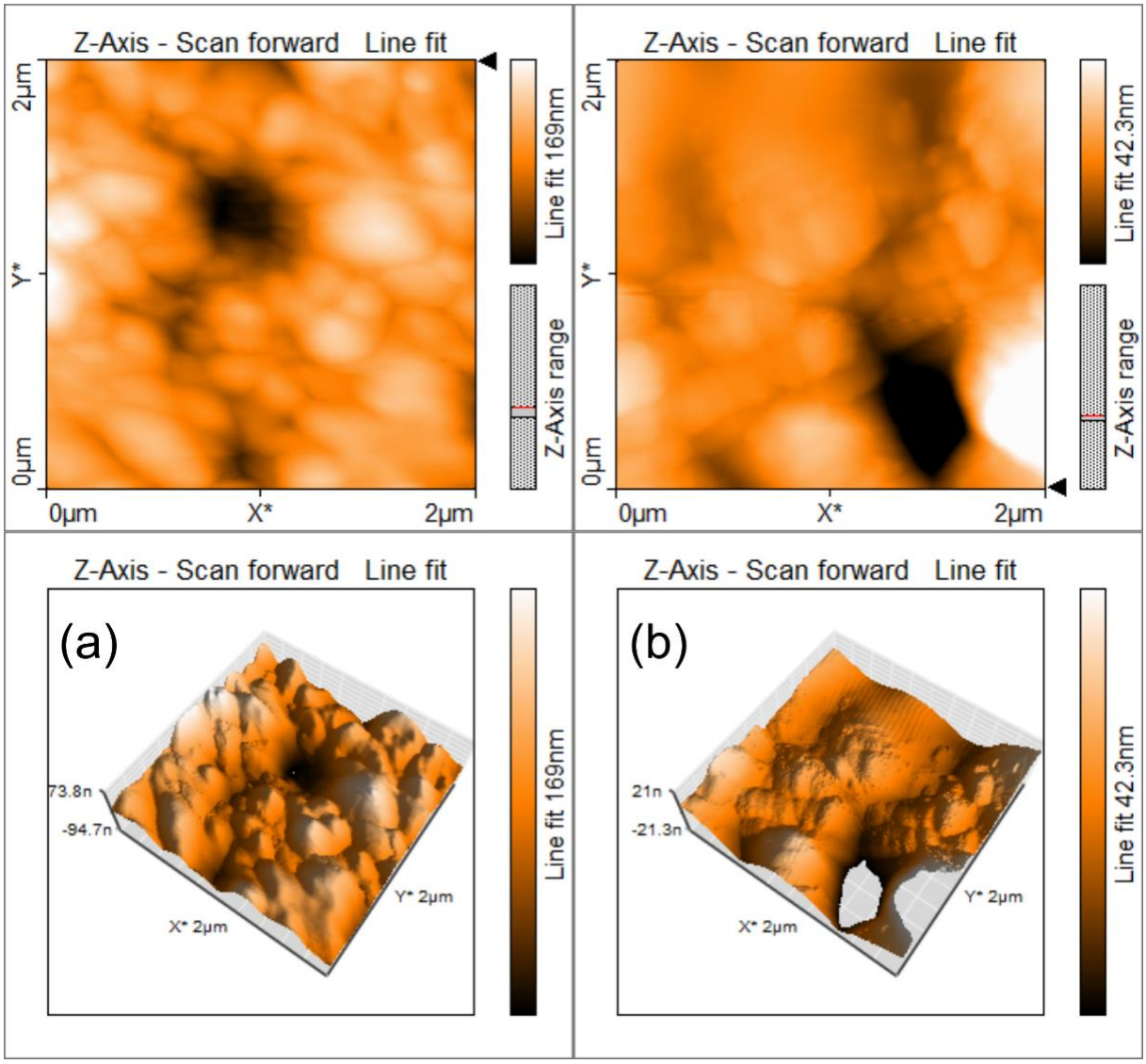

Figure 7. *AFM micrographs of selected samples; up: phase scan; down: 3D contour;* ***(a)*** *MS TiO_2-closed solar cell;* ***(b)*** *NR ZnO-closed solar cell.*

3.4. Specific characterisation of PSCs outside the scope of in-situ experiment – FIB-STEM

Utilisation of the high-end tool for preparing cross-sections enabled elucidation of the onset of the degradation. Prepared FIB lamellas were subjected to HAADF STEM microscopy. High Z-contrast imaging (the intensity is proportional to Z^2) enabled collecting of the suitable micrographs. Since the perovskite layer contains Pb as heavy element; the phase contrast in the HAADF image (**Figure 8a**) already indicates that the perovskite partially infiltrated the mesoporous TiO_2 layer. The infiltration was further confirmed by the EDS measurements. The EDS map was taken from the region indicated by the yellow rectangle in the HAADF figures. Both in the Pb and the I map, the infiltration into the TiO_2 was clearly observed; enhanced by white arrows.

For the NR ZnO-based closed cells the interface and grain boundaries perovskite problems were obvious (**Figure 8b**). Something had prevented the formation of a homogeneous and hole-free perovskite layer on top of the ZnO nanorods; the defect-forming tendency of ZnO has already been mentioned, but it was difficult to judge whether the incompatibility of surface energies or hydrophobicity presented an additional contribution. Moreover, an increased concentration of traps at the interface might lead to charge accumulation, which acts as an energy barrier, slightly reducing the overall electrical field being formed (open circuit voltage), and extracting current from the device **[42,43]**. However, the shunt resistance, which is usually indicative of traps and pinholes inside the film, had not drastically changed when switching from one ETL to the other. Furthermore, for ZnO-nanorod assembled devices, one can observe an S-shaped curve during forward scan in comparison to TiO_2 **(Figure 2)**. This phenomenon is usually related to the aforementioned issues, and its existence implies that the interface charge transport is the key limiting factor for this system **[44,45]**. Such behaviour does not come as a surprise for the ZnO nanostructure **[46,47]**, but the extent of the phenomenon is actually surprising. Actions have to be taken to further optimise this interface, i.e., different perovskite composition, surface treatments, deposition parameters, etc.

Spectroscopic-optical-surface-electrical analyses confirmed the successfulness of the synthesis and assembly. We confirm that fresh cells had the typical composition, without traces of the degradation products. On the other hand, those that were not analysed immediately upon exposure to atmospheric conditions, showed degradation traces and products. Generally, the cells were significantly different after degradation. Therefore, we were able to compare several factors.

The quadruple cation system responds very well to PSC functional performance, to stability in normal aging, and to stability under enhanced aging conditions, except in the case when nanostructured ZnO ETL is used. The negative degradation influence is obvious for certain compositions and levels of nanostructural organisation of ETLs. In the case of our ETLs, MS TiO_2 meets this limit, while NR ZnO does not. There might be a work around: resolving future challenges will require improved control over ZnO-nanorod growth, to avoid any defect-related repercussions in the perovskite layer. Nevertheless, even with such defects affecting the formation of a poor interface, the devices were still of comparable performance, and upon improving on those issues, one can expect the efficiency of ZnO-nanorods-fabricated devices to surpass those of mesoporous TiO_2. In conclusion, we are of the opinion that nanostructuring can increase efficiencies even for the combination of more complex perovskite absorbers and ZnO NR, provided the ZnO NR surface is passivated, for example, by titania coating in a core-shell configuration.

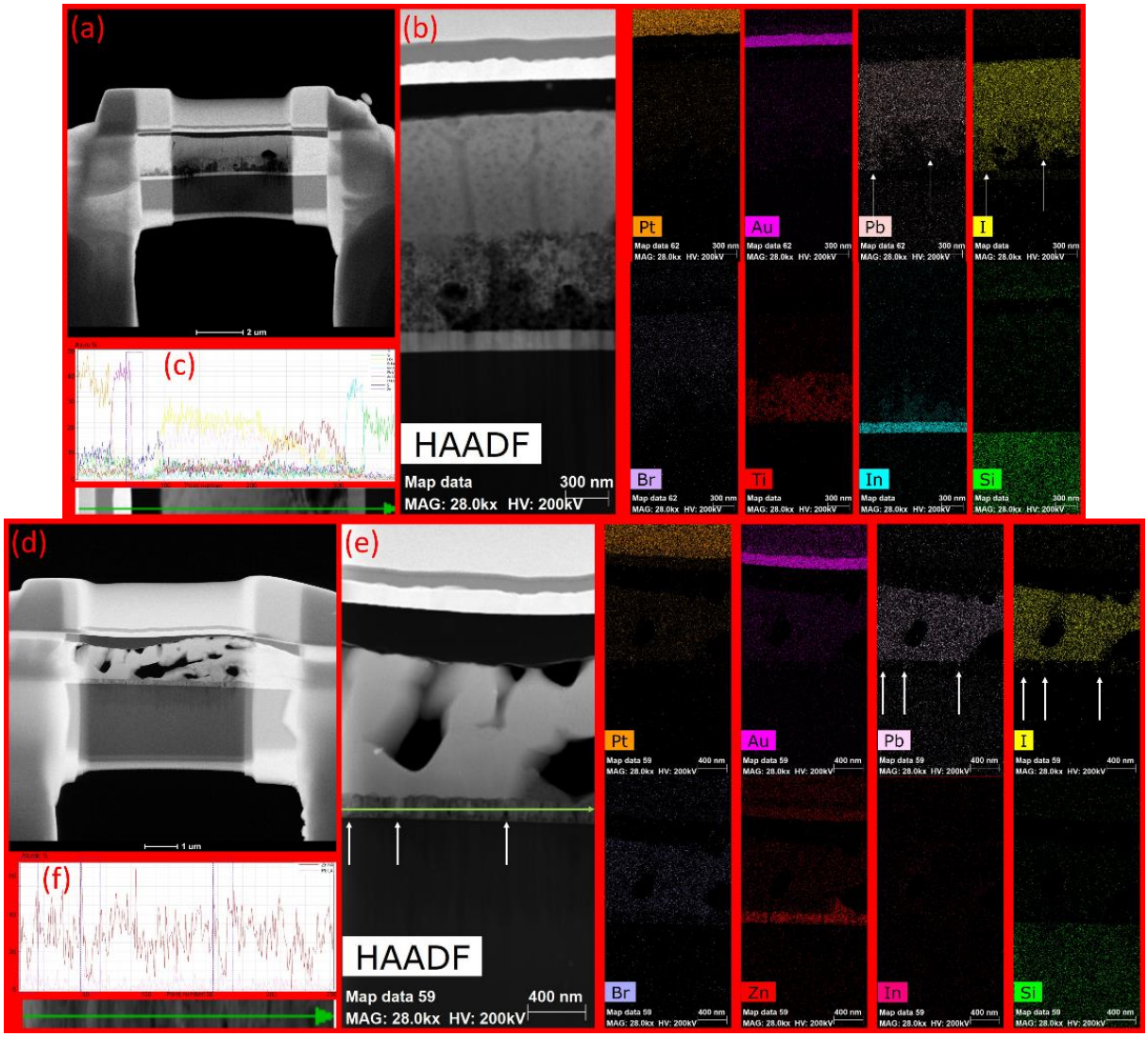

Figure 8. *FIB-STEM micrographs with EDS mapping;* ***(a)*** *STEM image of a lamella for MS TiO_2-closed cell;* ***(b)*** *HAADF-STEM with mapping for MS TiO_2-closed cell;* ***(c)*** *line profiles for MS TiO_2-closed cell;* ***(d)*** *STEM of lamella for NR ZnO-closed cell;* ***(e)*** *HAADF-STEM with mapping for NR ZnO-closed cell;* ***(f)*** *line profiles for NR ZnO-closed cell.*

Conclusions

Perovskite solar cells in n-i-p configuration comprising quadruple rubidium-caesium-methylammonium-formamidinium (Rb-Cs-MA-FA) in (lead iodide/bromide) perovskite were prepared and tested. To shed more light on the stability of the PSCs, we investigated the influence of mesostructured titania and zincite nanorods as nanostructured ETLs. We established a multi-technique in-situ setup comprising synchrotron grazing incidence diffraction and Raman spectroscopy as a function of the temperature and ambient under isothermal conditions for testing of the influence of the ETLs variation on degradation parameters of the quadruple PSCs.

It was found that the aging at ambient conditions, and enhanced aging under elevated temperature, affected the degradation of the samples differently. Preparing quadruple cation perovskites does generally increase the stability of PSCs from the point of view of perovskite absorber stability. In addition, increasing the complexity of the system affects the PSC performance, which inevitably leads to the different interfacing properties. In our case, the degradation results point to some issues in the PSCs. Despite the elaborate approach, GID, Raman, FTIR, FESEM, AFM, PCE, and IV could not determine the source of the issues, i.e., conventional morphology, chemical, electrical, and surface analysis indicated the extent of the degradation, but offered limited

insight into the route and the mechanisms behind the decomposition. For the case of nanostructured ETLs, a detailed insight into the ETL/absorber interface is necessary to allow discussion about the degradation route mechanisms.

FIB-STEM finally enabled the required insight into the absorber/ETL interface, to understand the lower efficiencies of the solar cells comprising the ZnO nanorod ETL. For the case of the nanostructured zincite, the perovskite absorber contained many voids, suggesting that the proposed quadruple perovskite absorber was not well compatible with ZnO NR ETL. The exchange of the ZnO NR ETL with MS TiO_2 increased the stability parameters. The lower performance of ZNR ETL incorporated into the perovskite layer can be assigned to a poorly formed interface due to "surface imperfections" of the nanorods. Optimization of the perovskite ZnO interface could make the nanostructured ZnO based PSC predominant over TiO_2 based devices.

Acknowledgement

This work has been funded by the projects **PZS-2019-02-1555** PV-WALL in Research Cooperability Program of the Croatian Science Foundation funded by the European Union from the European Social Fund under the Operational Programme Efficient Human Resources 2014-2020 (perovskite solar cells), **UIP-2019-04-2367** SLIPPERY-SLOPE of the Croatian Science Foundation (nanostructured titania and zincite constituents), **KK.01.2.1.02.0316** "The development of the technical solution for energy saving using VIS-transparent or semi-transparent and IR-reflective thin-films" by the European Regional Development Fund (ERDF) (characterisation of thin-films), **20190571** and **20190516** at Elettra Synchrotron, **ICM-2019-13220** in Ernst Mach program of the OeAD-GmbH, and **E210900588** in the EUSMI program. The group of prof Gregor Trimmel of the ICTM, NAWI Graz, the beamline scientists of the MCX beamline of the Elettra synchrotron, and FIB-STEM researchers of the Faculty of Science, University of Antwerp, are gratefully acknowledged for collaboration and instrument access. The financial sustenance of the University of Zagreb is gratefully acknowledged.

References

[1] J. P. Correa-Baena, M. Saliba, T. Buonassisi, M. Gratzel, A. Abate, W. Tress, A. Hagfeldt, Promises and challenges of perovskite solar cells, Science, 2017, 358, 739-744. doi: 10.1126/science.aam6323

[2] M. A. Green, A. Ho-Baillie, H. J. Snaith, The emergence of perovskite solar cells, Nature Photonics, 2014, 8, 506-514. doi: 10.1038/nphoton.2014.134

[3] J. Young Kim, J. W. Lee, H. S. Jung, H. Shin, N. G. Park, High-Efficiency Perovskite Solar Cells, Chem. Rev. 2020, 120, 7867-7918. doi: 10.1021/acs.chemrev.0c00107

[4] V. Gonzalez-Pedro, E. J. Juarez-Perez, W. S. Arsyad, E. M. Barea, F. Fabregat-Santiago, I. Mora-Sero, J. Bisquert, General working principles of $CH_3NH_3PbX_3$ perovskite solar cells, Nano Lett. 2014, 14, 888-893. doi: 10.1021/nl404252e

[5] A. B. Djurišić, F. Z. Liu, H.W. Tam, M.K. Wong, A. Ng, C. Surya, W. Chen, Z. B. He, Perovskite solar cells - An overview of critical issues, Prog. Quantum Electron, 2017, 53, 1-37. doi: 10.1016/j.pquantelec.2017.05.002

[6] X. Zhao, N. G. Park, Stability Issues on Perovskite Solar cells, Photonics, 2015, 2, 1139-1151. doi. 10.3390/photonics2041139

[7] K. M. Reza, A. Gurung, B. Bahrami, A. Haider Chowdhury, N. Ghimire, R. Pathak, S. I. Rahman, M. A. Rahman Laskar, K. Chen, R. S. Bobba, B. S. Lamsal, L. K. Biswas, Y. Zhou, Grain Boundary Defect Passivation in Quadruple Cation Wide-Bandgap Perovskite Solar Cells, Solar RRL, 2021, 5, 2000740. doi: 10.1002/solr.202000740

[8] P. Yadav, M. I. Dar, N. Arora, E. A: Alhabri, F. Giordano, S. M. Zakeeruddin, M. Gratzel, The role of rubidium in multiple-cation-based high-efficiency perovskite solar cells, Adv. Mat. 2017, 29, 17001077. doi: 10.1002/adma.201701077

[9] C. H. Ng, T. S. Ripolles, K. Hamada, S. H. Teo, H. N. Lim, J. Bisquert, S. Hayase, Tunable open circuit voltage by engineering inorganic caesium lead bromide/iodide perovskite solar cells, Sci. Rep. 2018, 8, 2482. doi: 10.1038/s41598-018-20228-0

[10] S. H. Turren-Cruz, A. Hagfeldt, M. Saliba, Methylammonium-free, high-performance, and stable perovskite solar cells on planar architecture, Science, 2018, 362, 449-453. doi: 10.1126/science.aat3583

[11] Y. Yu, C. Wang, C. R. Grice, N. Shrestha, D. Zhao, W. Liao, L. Guan, R. A. Awni, W. Meng, A. J. Cimaroli, Synergistic Effects of Lead Thiocyanate Additive and Solvent Annealing on the Performance of Wide-Bandgap Perovskite Solar Cells,. ACS Energy Lett. 2017, 2, 1177. doi: 10.1021/acsenergylett.7b00278

[12] M. Saliba, T. Matsui, K. Domanski, J.-Y. Seo, A. Ummadisingu, S. M. Zakeeruddin, J.-P. Correa-Baena, W. R. Tress, A. Abate, A. Hagfeldt, M. Gratzel, Incorporation of rubidium cations into perovskite solar cells improves photovoltaic performance, Science 2016, 354, 206-209. doi: 10.1126/science.aah5557

[13] A. Rajagopal, R. J. Stoddard, S. B. Jo, H. W. Hillhouse, A. K.-Y. Jen, Overcoming the Photovoltage Plateau in Large Bandgap Perovskite Photovoltaics, Nano Lett. 2018, 18, 3985-3993. doi: 10.1021/acs.nanolett.8b01480

[14] S. Gharibzadeh, B. Abdollahi Nejand, M. Jakoby, T. Abzieher,D. Hauschild, S. Moghadamzadeh, J. A. Schwenzer, P. Brenner,R. Schmager, A. A. Haghighirad, Record Open-Circuit Voltage Wide-Bandgap Perovskite Solar Cells Utilizing 2D/3D Perovskite Heterostructure, Adv. Energy Mater. 2019, 9, 1803699. doi: 10.1002/aenm.201803699

[15] M. Saliba, J. P. Correa-Baena, C. M. Wolff, M. Stolterfoht, N. Phung, S. Albrecht, D. Neher, A. Abate, How to make over 20% efficient perovskite solar cells in regular (n-i-p) and inverted (p-i-n) architectures, Chem. Mater. 2018, 30, 4193-4201. doi: 10.1021/acs.chemmater.8b00136

[16] A. Guerrero, J. You, C. Aranda, Y. Soo Kang, G. Garcia-Belmonte, H. Zhou, J. Bisquert, Y. Yang, Interfacial degradation of planar lead halide perovskite solar cells, ACS Nano, 2016, 10, 218-224. doi: 10.1021/acsnano.5b03687

[17] Q. Fu, X. Tang, B. Huang, T. Hu, L. Tan, L. Chen, Y. Chen, Recent progress on the long-term stability of pervoskite solar cells, Adv. Sci. 2018, 5, 1700387. doi: 10.1002/advs.201700387

[18] H. R. Mohseni, M. Dehghanipour, N. Dehghan, F. Tamaddon, M. Ahmadi, M. Sabet, A. Behjat, Enhancement of the photovoltaic performance and the stability of perovskite solar cells via the modification of electron transport layers with reduced graphene oxide/polyaniline composite, Sol. Ene. 2021, 213, 59-66. doi: 10.1016/j.solener.2020.11.017

[19] R. Irandoost, S. Soleimani-Amiri, Design and analysis of high efficiency perovskite solar cells with ZnO nanorods and plasmonic nanoparticles, Optik, 2020, 202, 163598. doi: 10.1016/j.ijleo.2019.163598

[20] J. He, T. Li, X. Liu, H. Su, Z. Ku, J. Zhong, F. Huang, Y. Peng, Yi.B. Cheng, Influence of phase transition on stability of perovskite solar cells under thermal cycling conditions, Sol. Ene. 2019, 188, 312-317.

[21] Z. Song, S.C. Watthage, A.B. Philips, B. L. Tompkins, R. J. Elingson, M. J. Heben, Impact of processing temperature and composition on the formation of methylammonium lead iodide perovskites, Chem. Mater. 2015, 27, 4612-4619. doi: 10.1021/acs.chemmater.5b01017

[22] G. Abdelmageed, C. Mackeen, K. Hellier, L. Jewell, L. Swymour, M. Tingwald, F. Bridges, J. Z. Zhang, S. Carter, Effect of temperature on light induced degradation in methylammonium lead iodide perovskite thin film and solar cells, Sol. Energy Mater. Sol. Cells, 2018, 174, 566-571. doi: 10.1016/j.solmat.2017.09.053

[23] A. F. Akbulatov, S.Yu Luchkin, L. A. Frolova, N. N. Dremova, K. L. Gerasimov, I. S. Zhidkov, D. V. Anokhin, E. Z. Kurmaev, K. J. Stevenson, P. A. Troshin, Probing the intrinsic thermal and photochemical stability of hybrid and inorganic lead halide perovskites, J. Phys. Chem. Lett. 2017, 8, 1211-1218. doi: 10.1021/acs.jpclett.6b03026
[24] N. Lkhdar, A. Hima, Electron transport material effect on performance of perovskite solar cells based on $CH_3NH_3GeI_3$, Opt. Mater. 2020, 99, 109517. doi: 10.1016/j.optmat.2019.109517
[25] K. Mahmood, S. Sarwar, M. T. Mehran, Current status of electron transport layers in perovskite solar cells: materials and properties, RSC ADV. 2017, 7, 17044-17062. doi: 10.1039/C7RA00002B
[26] J. Choi, S. Song, M. T. Horantner, H. J. Snaith, T. Park, Well-defined nanostructured, single-crystalline TiO2 electron transport layer for efficient planar perovskite solar cells, ACS Nano 2016, 10, 6029-6036. doi: 10.1021/acsnano.6b01575
[27] K. Mahmood, B. S. Swain, A. Amassian, Double-layered ZnO nanostructures for efficient perovskite solar cells, Nanoscale, 2014, 6, 14674-14678. doi: 10.1039/C4NR04383A
[28] V. Mandić, M. Plodinec, I. Kereković, K. Juraić, V. Janicki, D. Gracin, A. Gajović, A. Moguš-Milanković, M. G. Willinger, Tailoring anatase nanotubes for the photovoltaic device by the anodization process on behalf of microstructural features of titanium thin film, Sol. Energy Mater. Sol.Cells 2017, 168, 136-145. doi: 10.1016/j.solmat.2017.04.028
[29] V. J. Garcia, C. M. Pelicano, H. Yanagi, Low temperature-processed ZnO nanorods-TiO_2 nanoparticle composite as electron transporting layer for perovskite solar cells, Thin Solid Films 2018, 662, 70-75. doi: 10.1016/j.tsf.2018.07.039
[30] J. A. Alberola-Borras, R. Vidal, I. Mora-Sero, Evaluation of multiple cation/anion perovskite solar cells through life cycle assessment, Sustain. Energy Fuels, 2018, 2, 1600-1609. doi: 10.1039/C8SE00053K
[31] D. Wang, M. Wright, N. K. Elumalai, A. Uddin, Stability of perovskite solar cells, Sol. Energy Mater. Sol. Cells, 2016, 147, 255-275. doi: 10.1016/j.solmat.2015.12.025
[32] C.C. Boyd, R. Chaechaeron, T. Leijtens, M. D. McGehee, Understanding degradation mechanism and improving stability of perovskite photovoltaics, Chem. Rev. 2019, 119, 3418-3451. doi: 10.1021/acs.chemrev.8b00336
[33] A. Dualeh, P. Gao, S. Seok, M. K. Nazeeruddin, M. Gratzel, Thermal Behaviour of Methylammonium Lead-Trihalide Perovskite Photovoltaic Light Harvesters. Chem. Mater. 2014, 26, 6160–6164. doi: 10.1021/cm502468k
[34] T. Malinauskas, D. Tomkute-Luksiene, R. Sens, M. Daskeviciene, R. Send, H. Wonneberger, V. Jankauskas, I. Bruder, V. Getautis, Enhancing Thermal Stability and Lifetime of Solid-State Dye-Sensitized Solar Cells via Molecular Engineering of the Hole-Transporting Material Spiro-OMeTAD. ACS Appl. Mater.Interfaces 2015, 7, 11107–11116. doi: 10.1021/am5090385
[35] N. N. Shlenskaya, N. A. Belich, M. Gratzel, E. A. Goodilin, A. B. Tarasov, Light-Induced Reactivity of Gold and Hybrid Perovskite as a New Possible Degradation Mechanism in Perovskite Solar Cells. J. Mater. Chem. A 2018, 6, 1780–1786. doi: 10.1039/C7TA10217H
[36] J. Zhao, Y. Deng, H. Wei, X. Zheng, Z. Yu, Y. Shao, J. E. Shield, J. Huang, Strained Hybrid Perovskite Thin Films and Their Impact on the Intrinsic Stability of Perovskite Solar Cells. Sci. Adv. 2017, 3, No. eaa05616. doi: 10.1126/sciadv.aa05616
[37] F. U. Kosasih, C. Ducati, Characterising degradation of perovskite solar cells through in-situ and operando electron microscopy, Nano energy, 2018, 47, 243-256. doi: 10.1016/j.nanoen.2018.02.055
[38] M. Nazeri, M. Reza Golobostanfard, H. Kheirabadi, H. Abdizadeh, Sulfides as a new class of stable cost-effective materials compared to organic/inorganic hole transport materials for perovskite solar cells. Ceram Int. 48 (2022) 17995-18020. doi: 10.1016/j.ceramint.2022.03.163
[39] N. Li, Z. Zhu, C. C. Chueh, H. Liu, B. Peng, A. Petrone, X. Li, L. Wang, A. K. Y. Jen, Mixed cation FAxPEA1-xPbI3 with enhanced phase and ambient stability toward high-performance perovskite solar cells, Adv. Ener. Mat. 2017, 11, 1601307. doi: 10.1002/aenm.201601307
[40] S. Wieghold, J. P. Correa-Baena, L. Nienhaus, S. Sun, K. E. Shulenberger, Z. Liu, J. S. Tresback, S. S. Sin, M. G. Bawendi, T. Buonassisi, Precursor concentration affects grain size, crystalline orientation, and local performance in mixed-ion lead perovskite solar cells. ACS Appl. Energy Mat. 2018, 1, 6801-3808. doi: https://doi.org/10.1021/acsaem.8b00913
[41] S. Ruan, D. P. McMeekin, R. Fan, N. A.S. Webster, H. Ebendorff-Heidepriem, Y. B. Cheng, J. Lu, Y: Ruan, C. R. McNeill, Raman Spectroscopy of Formamidinium-Based Lead Halide Perovskite Single Crystals, J. Phys. Chem C 2020, 124,4,2265-2272. doi: 10.1021/acs.jpcc.9b08917
[42] B. Wu, K. Fu, N. Yantara, G. Xing, S. Sun, T.-C. Sum, N. Mathews, Charge Accumulation and Hysteresis in Perovskite-Based Solar Cells: An Electro-Optical Analysis. Adv. Energy. Mater. 2015, 5, 1500829, doi: 10.1002/aenm.201500829
[43] Y. Wang, H.-Y. Wang, M. Yu, L.-M. Fu, Y. Qin, J.-P. Zhang, X.-C. Ai, Trap-Limited Charge Recombination in Intrinsic Perovskite Film and Meso-Superstructured Perovskite Solar Cells and the Passivation Effect of Hole-Transport Material on Trap States, Phys. Chem. Chem. Phys. 2015,17, 29501-29506. doi: 10.1039/C5CP04360C
[44] Y. Shao, Z. Xiao, C. Bi et al. Origin and elimination of photocurrent hysteresis by fullerene passivation in $CH_3NH_3PbI_3$ planar heterojunction solar cells. Nat. Commun. 2014, 5, 5784 doi: 10.1038/ncomms6784
[45] B. Qi, J. Wang, Fill factor in organic solar cells, Phys. Chem. Chem. Phys. 2013, 15, 8972. doi: 10.1039/c3cp51383a
[46] T. H. Lee, J. W. Lee, C. Choi, S. Tan, C. Lee, Y. Zhao, Z. Dai, N. De Marco, S. J. Lee, S. H. Bae, Y. Yuan, H. M. Lee, Y. Huang, Y. Yang, Perovskite-polymer composite cross-linker approach for highly-stable and efficient perovskite solar cells, Nature Communications, 2019, 10,520. doi: 10.1038/s41467-019-08455-z
[47] S. Li, P. Zhang, Y. Wang, H. Sarvari, D. Liu, J. Wu, Y. Yang, Z. Wang, Z. D. Chen, Interface engineering of high efficiency perovskite solar cells based on ZnO nanorods using atomic layer deposition, Nano Research 2017, 10,1092–1103. doi: 10.1007/s12274-016-1407-0

Captions

Tables

Table 1. PSC sample degradation conditions and denomination.
Table 2. J/V characteristic of selected ZnO and TiO_2 closed solar cells.

Figures

Figure 1. (a) Scheme of the in-situ setup, and **(b)** Geometry of the n-i-p configuration of the solar cells comprising the NR ZnO, MS TiO_2, or ZnO-TiO_2 ETLs.
Figure 2. Summary of IV characteristics measurements for selected open cells; **(a)** NR ZnO-closed solar cell, and **(b)** MS TiO_2-closed solar cell, and MS TiO_2-diluted-closed solar cell.
Figure 3. In-situ RT degradation and thermally enhanced degradation, including RT relaxation: GID depth profiling at several incidence angles of the solar cell samples; **(a)** ZnO-based open solar cell; **(b)** ZnO-based closed solar cell; **(c)** TiO_2-based open solar cell; **(d)** TiO_2-based closed solar cell; **(e)** ZnO-TiO_2-based open solar cell; **(f)** ZnO-TiO_2-based closed solar cell.
Figure 4. Additionally, thermally enhanced degradation for closed NR ZnO-closed solar cell: GID depth profiling at several incidence angles of cells.
Figure 5. Summary of measurements for selected open/closed cells; NR ZnO, MS TiO_2 (pink and blue shaded areas show peak for N-H bonds); **(a)** ATR-FTIR; **(b)** micro-Raman spectroscopy.
Figure 6. FESEM micrographs of selected; **(a)** MS TiO_2-closed solar cell; **(b)** NR ZnO-closed solar cell.
Figure 7. AFM micrographs of selected samples; up: phase scan; down: 3D contour; **(a)** MS TiO_2-closed solar cell; **(b)** NR ZnO-closed solar cell.
Figure 8. FIB-STEM micrographs with EDS mapping; **(a)** STEM image of a lamella for MS TiO_2-closed cell; **(b)** HAADF-STEM with mapping for MS TiO_2-closed cell; **(c)** line profiles for MS TiO_2-closed cell; **(d)** STEM of lamella for NR ZnO-closed cell; **(e)** HAADF-STEM with mapping for NR ZnO-closed cell; **(f)** line profiles for NR ZnO-closed cell.